

Constraints on Dark Energy Models with Gamma-Ray Bursts Calibrated from the Observational $H(z)$ Data

Zihao Li^{*}, Bin Zhang[†] and Nan Liang[‡]

¹Key Laboratory of Information and Computing Science Guizhou Province, Guizhou Normal University, Guiyang, Guizhou 550025, China

²Joint Center for FAST Sciences Guizhou Normal University Node, Guiyang, Guizhou 550025, China

Accepted XXX. Received YYY; in original form ZZZ

ABSTRACT

We use a cosmology-independent method to calibrate gamma-ray burst (GRB) from the observational Hubble data (OHD) which obtained with the cosmic chronometers method. By using Gaussian Process to reconstruct OHD, we calibrate the Amati relation (E_p-E_{iso}) to construct a GRB Hubble diagram with the A118 data set, and constrain Dark Energy models in a flat space with the Markov Chain Monte Carlo numerical method. With the cosmology-independent GRBs at $1.4 < z \leq 8.2$ in the A118 data set and the Pantheon sample of type Ia supernovae (SNe Ia) at $0.01 < z \leq 2.3$, we obtained $\Omega_m = 0.398^{+0.028}_{-0.021}$, $h = 0.702^{+0.0035}_{-0.0035}$, $w = -1.33^{+0.14}_{-0.12}$, $w_a = -0.97^{+0.57}_{-0.57}$ for the flat CPL model at the 1σ confidence level. We find that the Λ CDM model is favoured respect to the w CDM model and the CPL model with the selection criteria.

Key words: Gaussian Process — Gamma-ray burst — Markov Chain Monte Carlo

1 INTRODUCTION

Gamma-ray bursts (GRBs) are the most intense bursts of high-energy gamma rays from cosmological space in a short period of time. At present, the maximum redshift of GRB can reach at $z \sim 9$ (Cucchiara et al. 2011), while the maximum redshift observed by SNe Ia is about $z \sim 2$ (Scolnic et al. 2018). Therefore, GRBs can be used to probe the universe at high-redshift beyond SNe Ia. The so-called Amati relation, which connects the spectral peak energy and the isotropic equivalent radiated energy (the E_p-E_{iso} correlation) of GRBs, has been proposed by Amati et al. (2002). Utilizing the Amati relation and/or other luminosity relations of GRB (Fenimore & Ramirez-Ruiz 2000; Norris et al. 2000; Ghirlanda et al. 2004a; Yonetoku et al. 2004; Liang & Zhang 2005; Firmani et al. 2006; Dainotti et al. 2008; Tsutsui et al. 2009a; Izzo et al. 2015; Xu et al. 2021; Hu et al. 2021; Wang et al. 2022; Liu et al. 2022a), the GRBs have been used as cosmic probe to study the evolutionary history of our universe and the properties of dark energy (Schaefer 2003; Dai et al. 2004; Ghirlanda et al. 2004b; Firmani et al. 2005; Xu et al. 2005; Liang & Zhang 2006; Wang & Dai 2006; Schaefer 2007; Amati et al. 2008; Wang 2008; Liang et al. 2008; Capozziello & Izzo 2008; Kodama et al. 2008; Tsutsui et al. 2009b; Cardone et al. 2009; Capozziello & Izzo 2010; Liang et al. 2010, 2011; Wei 2010; Wang & Dai 2011; Gao et al. 2012; Liu & Wei 2015; Wang et al. 2016; Demianski et al. 2017b; Amati et al. 2019; Khadka & Ratra 2020; Khadka et al. 2021; Luongo & Muccino 2020, 2021; Montiel

et al. 2021; Demianski et al. 2021; Cao et al. 2022a,b; Dainotti et al. 2022; Liu et al. 2022b; Liang et al. 2022). For reviews of GRB luminosity relations and their applications in cosmology, see e.g. Ghirlanda et al. (2006) and Dainotti & Amati (2018).

Due to the lack of a low-redshift sample, a cosmological model has been assumed to calibrate the GRB luminosity relation in the early cosmological studies (Dai et al. 2004). When using the model-dependent GRB data to constrain cosmological models, the so-called circularity problem is encountered (Ghirlanda et al. 2006). In order to avoid the circularity problem of GRB in cosmological applications, Liang et al. (2008) proposed a cosmological model-independent method to calibrate the luminosity relations of GRBs by using the SNe Ia data. The luminosity distances of the low-redshift GRB data to calibrate the GRB luminosity relations are directly from SNe Ia at the same redshift. Following the cosmology-independent calibration method from SNe Ia by the interpolation method (Liang et al. 2008) or by other similar approaches (Kodama et al. 2008; Cardone et al. 2009; Capozziello & Izzo 2010; Gao et al. 2012; Liu & Wei 2015; Izzo et al. 2015; Demianski et al. 2017a), the derived GRB data at high redshift can be used to constrain cosmological models by using the standard Hubble diagram method (Capozziello & Izzo 2008, 2009; Tsutsui et al. 2009b; Wei & Zhang 2009; Wei 2010; Liang et al. 2010, 2011; Demianski & Piedipalumbo 2011).

On the other hand, the simultaneous fitting method has also been proposed to alleviate the circularity problem, which constrain the coefficients and the relationship and the parameters of the cosmological model simultaneously (Amati et al. 2008; Li et al. 2008). However, a specific cosmological model is required for simultaneous fitting. Recently, Khadka & Ratra (2020) fitted the cosmolog-

* lizihao@gznu.edu.cn

† binzhang@gznu.edu.cn

‡ liangn@bnu.edu.cn

ical and GRB relation parameters simultaneously in six different cosmological models, and found that the Amati relation parameters are almost identical in all cosmological models. [Khadka et al. \(2021\)](#) compiled a data set of 118 GRBs (the A118 sample) from the total 220 GRBs (the A220 sample) with the smallest intrinsic dispersion to simultaneously derive the correlation and cosmological model parameter constraints. [Cao et al. \(2022a,b\)](#) used the A118 sample and the A220 sample to constrain cosmological model parameters simultaneously.

It should be noted that some systematic unknown biases of SNe Ia may propagate into the calibration results in the calibration procedure by using SNe Ia sample. [Amati et al. \(2019\)](#) proposed an alternative method to calibrate GRB correlations by using the observational Hubble data (OHD) at $z < 1.975$ through the Bézier parametric curve and built up a Hubble diagram consisting of 193 GRBs. Following this method from OHD fitted by the Bézier parametric to calibrate GRBs ([Amati et al. 2019](#)), [Montiel et al. \(2021\)](#) calibrate the Amati relation from the Fermi-GBM catalogue (74 GRBs) with the OHD at $z < 1.43$ to approximate the cosmic expansion. [Luongo & Muccino \(2021\)](#) used three machine learning treatments to get the mock data from differential Hubble rate points that calibrated the GRB correlations. [Luongo & Muccino \(2022\)](#) proposed a model-independent calibration of GRB correlations in non-flat cosmology based on the most updated OHD and baryonic acoustic oscillations (BAO). [Muccino et al. \(2022\)](#) calibrated the Amati relation from 1000 simulated OHD points by means of the Bézier polynomial technique to constrain the transition redshift.

More recently, [Liu et al. \(2022a\)](#) propose the improved Amati relations with the possible evolutionary effects via a powerful statistical tool called copula, and calibrated the copula relations from SNe Ia by the interpolation method to constrain cosmological models ([Liu et al. 2022b](#)). [Liang et al. \(2022\)](#) calibrate the Amati relation with the A220 sample and the A118 sample by using a Gaussian process from SNe Ia and constrain on the Λ CDM model and the w CDM model in flat space with GRBs at high redshift and 31 OHD, which are consistent with those from fitting the coefficients of the Amati relation and the cosmological parameters simultaneously.

In this paper, we plan to calibrate Amati relation with the A118 GRB data ([Khadka et al. 2021](#)) from the latest OHD by the Gaussian Process at low redshift, and obtain the GRB Hubble diagram at high redshift. Combined GRB data at $1.4 < z \leq 8.2$ with the Pantheon SNe Ia sample ([Scolnic et al. 2018](#)), we constrain Dark Energy (DE) models in a flat space with the Markov Chain Monte Carlo (MCMC) numerical method. Finally, we compare the DE models with the selection criteria.

2 CALIBRATION OF AMATI RELATION AT LOW-REDSHIFT

A Gaussian process is a non-parametric reconstruction for smoothing data by fully Bayesian approach, which has been widely applied to the field of cosmology ([Seikel et al. 2012a,b](#); [Lin et al. 2018](#); [Li et al. 2021](#); [Benisty 2021](#); [Benisty et al. 2022](#)). In this work, we use the newly OHD for reconstruction by the Gaussian Process to calibrate Amati relation at low redshift. Following [Seikel et al. \(2012a\)](#), we use the squared exponential covariance function for the advantage is that it is infinitely differentiable to reconstruct a function, which is given by

$$k(z, \tilde{z}) = \sigma_f^2 \exp \left[-\frac{(z - \tilde{z})^2}{2l^2} \right]. \quad (1)$$

Table 1. The latest OHD and their 1σ errors obtained with the CC method.

$H(z)$	z	$\sigma_{H(z)}$	REFERENCES
69	0.09	12	Jimenez et al. (2003)
83	0.17	8	Simon et al. (2005)
77	0.27	14	
95	0.4	17	
117	0.9	23	
168	1.3	17	
177	1.43	18	
140	1.53	14	
202	1.75	40	
97	0.48	62	Stern et al. (2010)
90	0.88	40	
75	0.1791	4	Moresco et al. (2012)
75	0.1993	5	
83	0.3519	14	
104	0.5929	13	
92	0.6797	8	
105	0.7812	12	
125	0.8754	17	
154	1.037	20	
69	0.07	19.6	Zhang et al. (2014)
68.6	0.12	26.2	
72.9	0.2	29.6	
88.8	0.28	36.6	
160	1.363	33.6	Moresco et al. (2015)
186.5	1.965	50.4	
83	0.3802	13.5	Moresco et al. (2016)
77	0.4004	10.2	
87.1	0.4247	11.2	
92.8	0.4497	12.9	
80.9	0.4783	9	
89	0.47	49.6	Ratsimbazafy et al. (2017)
98.8	0.75	33.6	Borghì et al. (2022)
113.1	0.80	28.5	Jiao et al. (2022)

Here the hyperparameter σ_f and l can be optimized by maximizing the marginal likelihood. We use public python package GaPP¹ to reconstruct OHD at low redshift.

The model-independent OHD have unique advantages to calibrated GRBs in a model-independent way ([Amati et al. 2019](#)). OHD can be obtained with the cosmic chronometers (CC) method, which related the evolution of differential ages of passive galaxies at different redshifts without assuming any cosmological model ([Jimenez & Loeb 2002](#)),

$$H(z) = -\frac{1}{1+z} \frac{dz}{dt}. \quad (2)$$

Applying the CC approach to the passively evolving galaxies from the luminous red galaxy (LRG) sample, 11 $H(z)$ data in the range $z \leq 1.8$ were obtained ([Jimenez et al. 2003](#); [Simon et al. 2005](#); [Stern et al. 2010](#)). Based on another analysis, [Moresco et al. \(2012, 2015, 2016\)](#) obtained 15 additional OHD in the range $0.179 \leq z \leq 1.975$. With a full-spectrum fitting technique, [Zhang et al. \(2014\)](#) determined 4 additional estimates of OHD at $z < 0.3$, and [Ratsimbazafy et al. \(2017\)](#) obtained one point at $z = 0.47$, respectively. These 31 OHD have been widely used for cosmological purposes ([Capozziello, D'Agostino, & Luongo 2018](#); [Amati et al. 2019](#); [Li et al. 2020](#); [Montiel et al. 2021](#); [Liu et al. 2022b](#); [Liang et al. 2022](#)).

¹ <https://github.com/astrobengaly/GaPP>

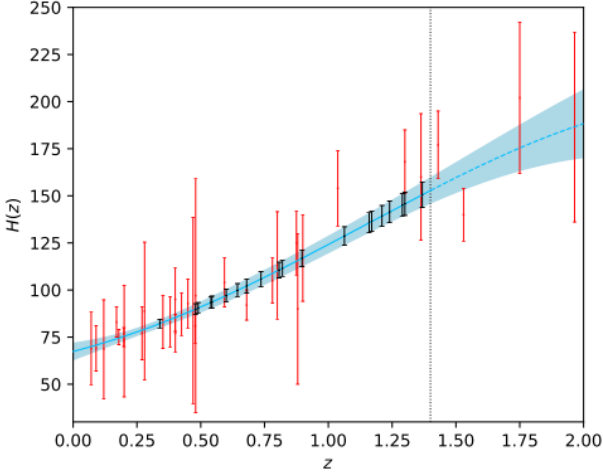


Figure 1. The reconstructed results from OHD through GaPP. The blue curves present the reconstructed function with the 1σ uncertainty. The results of GRBs at $z < 1.4$ (black dots) are reconstructed from OHD (red dots) through the Gaussian process. The black dashed line denotes $z = 1.4$.

More recently, [Borghi et al. \(2022\)](#) explore a new approach to obtain a new OHD at $z = 0.75$. [Jiao et al. \(2022\)](#) proposed a similar approach to obtain a new point at $z = 0.80$. For reviews of recent progress of OHD, see e.g. [Moresco et al. \(2022\)](#). The latest OHD obtained with the CC method are summarized in Table 1.² According to the analysis of [Moresco et al. \(2020\)](#) that OHD was carried out through simulations in the redshift range $0 < z < 1.5$, [Montiel et al. \(2021\)](#) calibrated the Amati relation with OHD at $z < 1.43$. In order to compare with the previous analyses ([Liu et al. 2022b](#); [Liang et al. 2022](#)), we used a subsample of Hubble parameter with a redshift cutoff at $z = 1.4$, which including 28 points. For GRB sample, we use the A118 GRB data set with the higher qualities appropriate for cosmological purposes in the A220 GRB data set ([Khadka et al. 2021](#)). There are 20 GRBs at low redshift $z < 1.4$ in the A118 GRB sample. The reconstructed results from the Gaussian process with the 1σ uncertainty from OHD are plotted in Figure 1.

The Amati relation ([Amati et al. 2002](#)) connects the spectral peak energy (E_p) and the isotropic equivalent radiated energy (E_{iso}), which can be expressed as

$$y = a + bx \quad (3)$$

where $y \equiv \log_{10} \frac{E_{\text{iso}}}{1 \text{erg}}$, $x \equiv \log_{10} \frac{E_p}{300 \text{keV}}$, a and b are free coefficients needing to be calibrated from the GRBs observed data in the formula. E_{iso} and E_p can be respectively expressed as:

$$E_{\text{iso}} = 4\pi d_L^2(z) S_{\text{bolo}} (1+z)^{-1}, \quad E_p = E_p^{\text{obs}} (1+z) \quad (4)$$

where E_p^{obs} is the observational value of GRB spectral peak energy and S_{bolo} is observational value of bolometric fluence, both E_p^{obs} and S_{bolo} can be observable. The luminosity distance can be

² Considering these two measurements are not fully independent and their covariance is not clear, [Zhang et al. \(2022\)](#) only use the point [Jiao et al. \(2022\)](#), which taking advantage of the $1/\sqrt{2}$ fraction of systematic uncertainty, with other 31 OHD to calibrate of HII Galaxies. In this work, we also use the 31 OHD and the point [Jiao et al. \(2022\)](#). One could either use the data from [Borghi et al. \(2022\)](#) alternatively.

Table 2. Calibration results (the intercept a , the slope b , and the intrinsic scatter σ_{int}) of the Amati relation in the A118 GRB sample at $z < 1.4$.

a	b	σ_{int}
$52.87^{+0.11}_{-0.11}$	$1.00^{+0.21}_{-0.21}$	$0.49^{+0.06}_{-0.011}$

calculated by the reconstructed OHD at the redshift of GRBs³

$$d_L^{\text{GaPP}} = c(1+z) \int_0^z \frac{dz'}{H(z')} \quad (5)$$

here the derivative $H(z)$ at redshift z can be reconstructed with OHD by GaPP at the redshift of GRBs.

The parameters of Amati relation a and b can be fitted through GRBs sample data with $z < 1.4$ by using the likelihood function method ([D'Agostini 2005](#))

$$\mathcal{L}(\sigma, a, b) \propto \prod_{i=1}^{N_1} \frac{1}{\sigma^2} \times \exp \left[-\frac{[y_i - y(x_i, z_i; a, b)]^2}{2\sigma^2} \right] \quad (6)$$

Here $\sigma = \sqrt{\sigma_{\text{int}}^2 + \sigma_{y,i}^2 + b^2 \sigma_{x,i}^2}$, in which σ_{int} means the intrinsic scatter. $\sigma_y = \frac{1}{\ln 10} \frac{\sigma_{E_{\text{iso}}}}{E_{\text{iso}}}$, $\sigma_{E_{\text{iso}}} = 4\pi d_L^2 \sigma_{S_{\text{bolo}}} (1+z)^{-1}$ is the error magnitude of isotropic equivalent radiated energy and $\sigma_{S_{\text{bolo}}}$ means the error magnitude of bolometric fluence, $\sigma_x = \frac{1}{\ln 10} \frac{\sigma_{E_p}}{E_p}$, here σ_{E_p} is the error magnitude of the spectral peak energy, and $N_1 = 20$ means the number of low red-shift GRBs in A118 data set. We implement Markov Chain Monte Carlo (MCMC) by using the python package emcee ([Foreman-Mackey et al. 2013](#)), which is optimized on the basis of Metropolis-Hastings algorithm. The calibrated results (the intercept a , the slope b and the intrinsic scatter σ_{int}) in the A118 GRB sample at $z < 1.4$ are summarized in Table 2. We find that the results are consistent with previous analyses that obtained in [Liang et al. \(2022\)](#); [Liu et al. \(2022b\)](#) using GaPP and interpolation from SNe Ia at $z < 1.4$.

3 GRB HUBBLE DIAGRAM AND CONSTRAINTS ON DE MODELS

Assuming the calibration results of the Amati relation at $z < 1.4$ are valid at high redshift, we can derive the luminosity distances of GRBs at $z > 1.4$ and build the GRB Hubble diagram, which is plotted in Figure 3. The uncertainty of GRB distance modulus with the Amati relation can be expressed as

$$\sigma_{\mu}^2 = \left(\frac{5}{2} \sigma_{\log \frac{E_{\text{iso}}}{1 \text{erg}}} \right)^2 + \left(\frac{5}{2 \ln 10} \frac{\sigma_{S_{\text{bolo}}}}{S_{\text{bolo}}} \right)^2 \quad (7)$$

where

$$\sigma_{\log \frac{E_{\text{iso}}}{1 \text{erg}}}^2 = \sigma_{\text{int}}^2 + \left(\frac{b}{\ln 10} \frac{\sigma_{E_p}}{E_p} \right)^2 + \sum \left(\frac{\partial y(x; \theta_c)}{\partial \theta_i} \right)^2 C_{ii} \quad (8)$$

here $\theta_c = \sigma_{\text{int}}, a, b$, and C_{ii} means the diagonal element of the covariance matrix of these fitting coefficients.

We use the GRB data in the Hubble diagram at $z > 1.4$ with

³ For the recent Planck results ([Planck Collaboration 2020](#)) favor a flat spatial curvature, we consider a flat space in this work. However, recently works constrain nonspatially flat models with GRBs and results are promising [Luongo & Muccino \(2022\)](#)

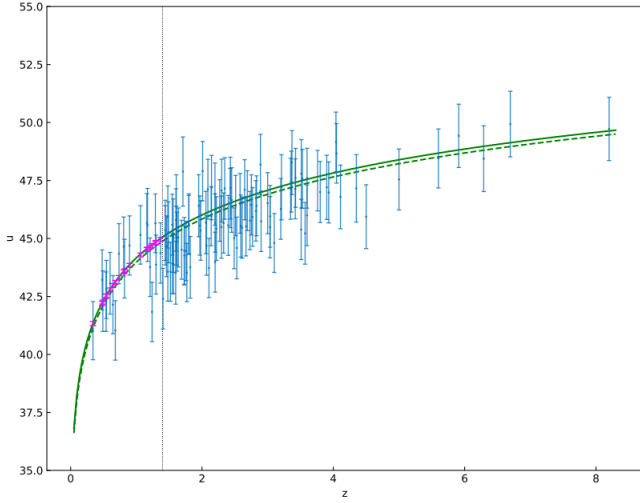


Figure 2. GRB Hubble diagram with the A118 data set. GRBs at $z < 1.4$ were obtained by a Gaussian process from the OHD data (purple points), while GRBs with $z > 1.4$ (blue points) were obtained by the Amati relation and calibrated with A118 at $z < 1.4$. The solid green curve is the CMB standard distance modulus with $H_0 = 67.36 \text{ km s}^{-1} \text{ Mpc}^{-1}$, $\Omega_m = 0.315$ (Plank Collaboration 2020), and the green long dotted curve is the SNIa standard distance modulus with $H_0 = 74.3 \text{ km s}^{-1} \text{ Mpc}^{-1}$, $\Omega_m = 0.298$ (Scolnic et al. 2018). The black dashed line denotes $z = 1.4$.

the Pantheon sample (Scolnic et al. 2018) to constrain cosmological models. The χ^2 for the distance modulus can be expressed as

$$\chi^2_{\mu} = \sum_{i=1}^N \left[\frac{\mu_{\text{obs}}(z_i) - \mu_{\text{th}}(z_i; p, H_0)}{\sigma_{\mu_i}} \right]^2. \quad (9)$$

Here μ_{obs} is the observational value of distance modulus and its error σ_{μ_i} , and μ_{th} is the theoretical value of distance modulus calculated from the cosmological model, p represents the cosmological parameters. The theoretical distance modulus of DE models can be calculated as

$$\mu = 5 \log \frac{d_L}{\text{Mpc}} + 25 = 5 \log_{10} D_L - \mu_0, \quad (10)$$

where $\mu_0 = 5 \log_{10} h + 42.38$, $h = H_0/(100 \text{ km/s/Mpc})$, H_0 is the Hubble constant. For a flat space, the unanchored luminosity distance D_L can be calculated by

$$D_L \equiv H_0 d_L = (1+z) \int_0^z \frac{dz'}{E(z')}, \quad (11)$$

where $E(z) = [\Omega_M(1+z)^3 + \Omega_{\text{DE}}X(z)]^{1/2}$, and $X(z) = \exp[3 \int_0^z \frac{1+w(z')}{1+z'} dz']$, which is determined by the choice of the specific dark energy (DE) model. We consider three DE models in a flat space, the Λ CDM model with dark energy EoS $w = -1$, the w CDM model with a constant Equation of State (EoS), and the Chevallier-Polarski-Linder (CPL) model (Chevallier & Polarski 2001; Linder 2003) in which dark energy evolving with redshift as a parametrization EoS, $w = w_0 + w_a z/(1+z)$.

$$X(z) = \begin{cases} 1, & \Lambda\text{CDM} \\ (1+z)^{3(1+w_0)}, & w\text{CDM} \\ (1+z)3(1+w_0+w_a)e^{-\frac{3w_a z}{1+z}}, & \text{CPL} \end{cases} \quad (12)$$

The Pantheon sample contains 1048 SNe spanning the redshift

range $0.01 < z < 2.3$, with the observed distance modulus of SNe given by (Scolnic et al. 2018)

$$m_{\text{SN}} = m_{\text{B}}^* - M + \alpha X_1 - \beta C + \Delta_M + \Delta_B, \quad (13)$$

where m_{B}^* is the observed peak magnitude in rest frame B-band, M is the absolute magnitude, X_1 is the time stretching of the light-curve, C is the SNe color at maximum brightness; α, β are nuisance parameters which should be fitted simultaneously with the cosmological parameters, Δ_M is a distance correction based on the host galaxy mass of the SN, and Δ_B is a distance correction based on predicted biases from simulations. The Pantheon data set is calibrated using the BEAMS with Bias Corrections (BBC) method (Kessler & Scolnic 2017), and the corrected apparent magnitude for all the SNe have been reported in Scolnic et al. (2018).

$$m_{\text{B,corr}}^* = m_{\text{B}}^* + \alpha X_1 - \beta C + \Delta_M + \Delta_B, \quad (14)$$

Following Liu et al. (2022b), we set the absolute magnitude to be $M = -19.36$ (Gomez-Valent 2022) in our analysis to obtain the distance modulus of SNe Ia.

The cosmological parameters can be fitted by using the minimization χ^2 method through MCMC method. The total χ^2 with the joint data of GRB+SNe can be expressed as $\chi^2_{\text{total}} = \chi^2_{\text{GRB}} + \chi^2_{\text{SN}}$. The python package emcee (Foreman-Mackey et al. 2013) is used to constrain DE models. Constraints only with 98 GRBs (A118) $z > 1.4$ are shown in Figure 3 (Λ CDM), Figure 4 (w CDM) and Figure 5 (CPL), which are summarized in Table 3. With 98 GRBs at $1.4 < z \leq 8.2$, we obtain $\Omega_m = 0.51^{+0.16}_{-0.33}$, $h = 0.771^{+0.096}_{-0.16}$ for the flat Λ CDM model, $\Omega_m = 0.50^{+0.25}_{-0.33}$, $h = 0.744^{+0.076}_{-0.16}$, $w = -0.95^{+0.75}_{-0.48}$ for the flat w CDM model at the 1σ confidence level. These results for the flat Λ CDM and the flat w CDM model are consistent with previous analyses that obtained in Liang et al. (2022) using GaPP from SNe Ia at $z < 1.4$ by setting $H_0 = 70 \text{ km s}^{-1} \text{ Mpc}^{-1}$ for the cases only with GRBs. The joint results from 98 GRBs (A118) $z > 1.4$ with 1048 SNe Ia are shown in Figure 6 (Λ CDM), Figure 7 (w CDM) and Figure 8 (CPL), which are summarized in Table 3. With 98 GRBs at $1.4 < z < 8.2$ in the A118 sample and 1048 SNe Ia, we obtained $\Omega_m = 0.292^{+0.012}_{-0.012}$ and $h = 0.696^{+0.002}_{-0.0029}$ for the flat Λ CDM model, and $\Omega_m = 0.375^{+0.031}_{-0.024}$, $h = 0.703^{+0.004}_{-0.004}$, $w = -1.35^{+0.14}_{-0.13}$ for the flat w CDM model, which are consistent with previous analyses that obtained in Liang et al. (2022) using GaPP from SNe Ia at $z < 1.4$.

For the flat CPL model with 98 GRBs $z > 1.4$, we obtained $\Omega_m = 0.53^{+0.24}_{-0.31}$, $h = 0.750^{+0.08}_{-0.16}$, $w = -0.91^{+0.88}_{-1.00}$, $w_a = -0.998^{+0.57}_{-0.57}$; with 98 GRBs $z > 1.4$ and 1048 SNe Ia, we obtained $\Omega_m = 0.398^{+0.028}_{-0.021}$, $h = 0.702^{+0.0035}_{-0.0035}$, $w = -1.33^{+0.14}_{-0.12}$, $w_a = -0.97^{+0.57}_{-0.57}$ for the flat CPL model at the 1σ confidence level, which favor a possible DE evolution ($w_a \neq 0$) at the $1-\sigma$ confidence region for both cases.

In order to compare the different cosmological models, we compute the values of the Akaike information criterion (AIC; Akaike et al. (1974, 1981)) and the Bayesian information criterion (BIC; Schwarz et al. (1978)), respectively.

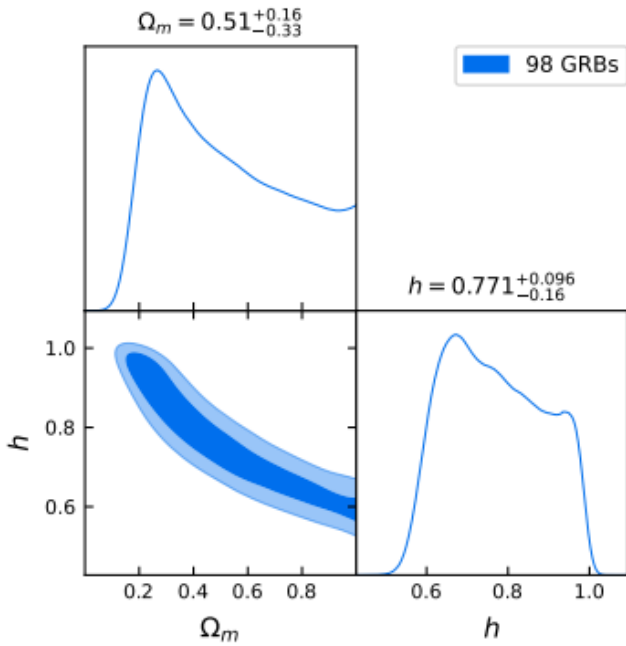
$$\text{AIC} = 2p - 2 \ln(\mathcal{L}) \quad (15)$$

$$\text{BIC} = p \ln N - 2 \ln(\mathcal{L}) \quad (16)$$

where \mathcal{L} is the maximum value of the likelihood function, p is the number of free parameters in a model, and N is the number of data. The value of ΔAIC and ΔBIC , which denotes the difference between AIC and BIC with respect to the reference model (the Λ CDM model) are summarized in Table 3. For the value of ΔAIC

Table 3. Joint constraints on parameters of Ω_m , h , w_0 and w_a for the flat Λ CDM model, the flat w CDM model, and the CPL model with 98 GRBs ($z \lesssim 1.4$) + 1048 SNe.

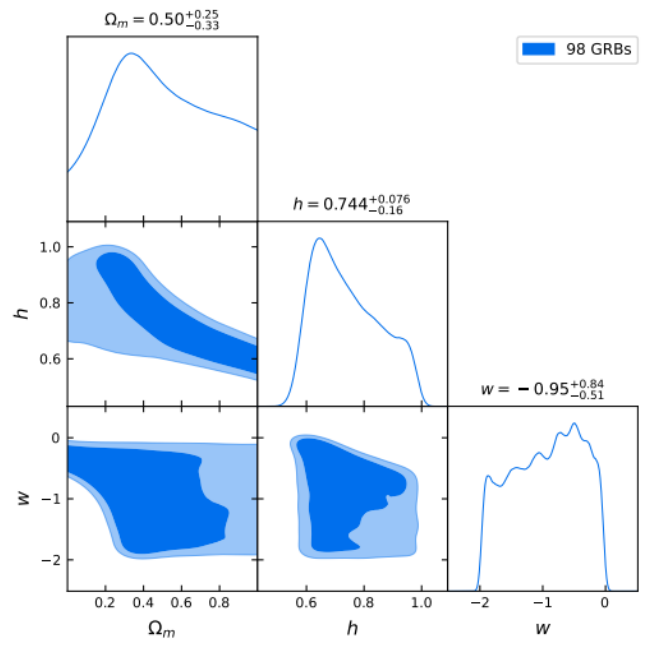
Models	Data Set	Ω_m	h	w_0	w_a	$-2 \ln \mathcal{L}$	ΔAIC	ΔBIC
Λ CDM	98 GRBs	$0.51^{+0.16}_{-0.33}$	$0.771^{+0.096}_{-0.16}$	-	-	56.053	-	-
w CDM	98 GRBs	$0.50^{+0.25}_{-0.33}$	$0.744^{+0.076}_{-0.16}$	$-0.95^{+0.84}_{-0.51}$	-	55.608	1.554	4.139
CPL	98 GRBs	$0.53^{+0.24}_{-0.31}$	$0.750^{+0.08}_{-0.16}$	$-0.91^{+0.86}_{-1.00}$	$-0.998^{+0.57}_{-0.57}$	55.728	3.675	8.845
Λ CDM	98 GRBs + 1048SNe	$0.292^{+0.012}_{-0.012}$	$0.696^{+0.002}_{-0.002}$	-	-	1104.768	-	-
w CDM	98 GRBs + 1048SNe	$0.375^{+0.031}_{-0.024}$	$0.703^{+0.004}_{-0.004}$	$-1.35^{+0.14}_{-0.13}$	-	1097.714	5.054	0.010
CPL	98 GRBs + 1048SNe	$0.398^{+0.028}_{-0.021}$	$0.702^{+0.0035}_{-0.0035}$	$-1.33^{+0.14}_{-0.12}$	$-0.97^{+0.57}_{-0.57}$	1097.619	3.148	6.94


Figure 3. Constraints on parameters of Ω_m , h for the flat Λ CDM model with 98 GRBs at $z \lesssim 1.4$.

and ΔBIC , $0 < \Delta\text{AIC}(\Delta\text{BIC}) < 2$ indicates difficulty in preferring a given model, $2 < \Delta\text{AIC}(\Delta\text{BIC}) < 6$ means mild evidence against the given model, and $\Delta\text{AIC}(\Delta\text{BIC}) > 6$ suggests strong evidence against the model. We find that the results of ΔAIC and ΔBIC indicate that the Λ CDM model is favoured respect to the w CDM model and the CPL model, which are consistent with the previous analyses (Amati et al. 2019) obtained from the 193 GRBs by using the OHD at $z < 1.975$ through the Bézier parametric curve combined with 740 SNe Ia.

4 CONCLUSIONS AND DISCUSSIONS

In this paper, we use the Gaussian process to calibrate the Amati relation from OHD and obtain the GRB Hubble diagram with the A118 sample. With 98 GRBs at $1.4 < z < 8.2$ in the A118 sample and 1048 SNe Ia, we obtained $\Omega_m = 0.292^{+0.012}_{-0.012}$ and $h = 0.696^{+0.002}_{-0.0029}$ for the flat Λ CDM model, and $\Omega_m = 0.375^{+0.031}_{-0.024}$, $h = 0.703^{+0.004}_{-0.004}$, $w = -1.35^{+0.14}_{-0.13}$ for the flat w CDM model, and $\Omega_m = 0.398^{+0.028}_{-0.021}$, $h = 0.702^{+0.0035}_{-0.0035}$, $w = -1.33^{+0.14}_{-0.12}$, $w_a = -0.97^{+0.57}_{-0.57}$ for the flat CPL model at the 1σ confidence level, which favor a possible DE evolution ($w_a \neq 0$) at the 1σ confidence region for both cases. We find that the results of ΔAIC and ΔBIC indicate


Figure 4. Constraints on parameters of Ω_m , h , and w_0 for the flat w CDM model with 98 GRBs at $z \lesssim 1.4$.

that the Λ CDM model is favoured respect to the w CDM model and the CPL model. In order to compare with simultaneous fitting method, we also use GRB data sets of A118 sample and SNe Ia to fit the coefficients of the Amati relation (a , b , σ_{int}) and the cosmological parameters (Ω_m , h , w , and w_a) simultaneously for the flat Λ CDM model, the flat w CDM model and the flat CPL model. It is found that the simultaneous fitting results are consistent with those obtained from the low-redshift calibration method.

It should be notice that GRB luminosity relations can be calibrated by using other observations, besides the calibration method by using SN Ia and OHD. For examples, Wang & Wang (2019) used the mock gravitational waves (GWs) catalog as standard sirens to calibrate GRB luminosity correlations. Dai et al. (2021) calibrated GRBs from quasar sample at $0.5 < z < 5.5$ which divided into several subsamples with different redshift bins, and found that the Amati relation shows no evolution with redshift. Gowri & Shantanu (2022) used the angular diameter distances of 38 galaxy clusters to circumvent the circularity problem in the Amati relation. Moreover, whether the GRB relations are redshift dependent or not is still under debate (Khadka et al. 2021; Dai et al. 2021; Tang et al. 2021; Liu et al. 2022a). Recently, Wang et al. (2022) use a tight correlation between the plateau luminosity and the end time of the plateau in the X-ray afterglows out to the redshift $z = 5.91$. Jia et al. (2022)

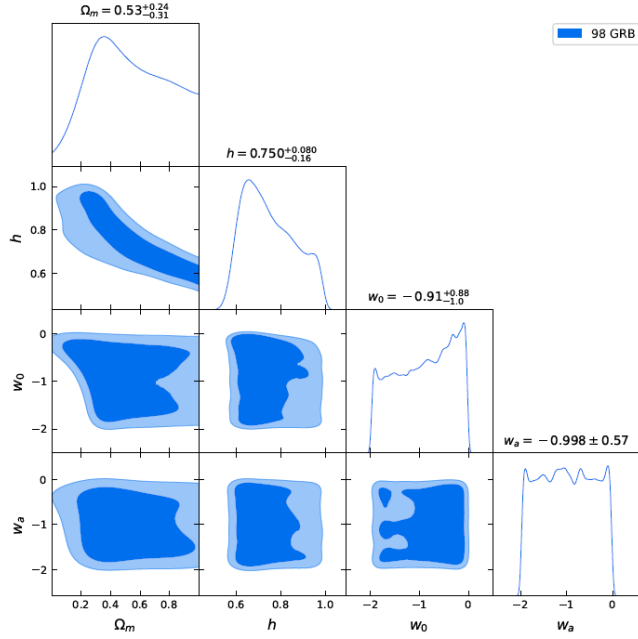


Figure 5. Constraints on parameters of Ω_m , h , w_0 and w_a for the flat CPL model with 98 GRBs at $z_i 1.4$.

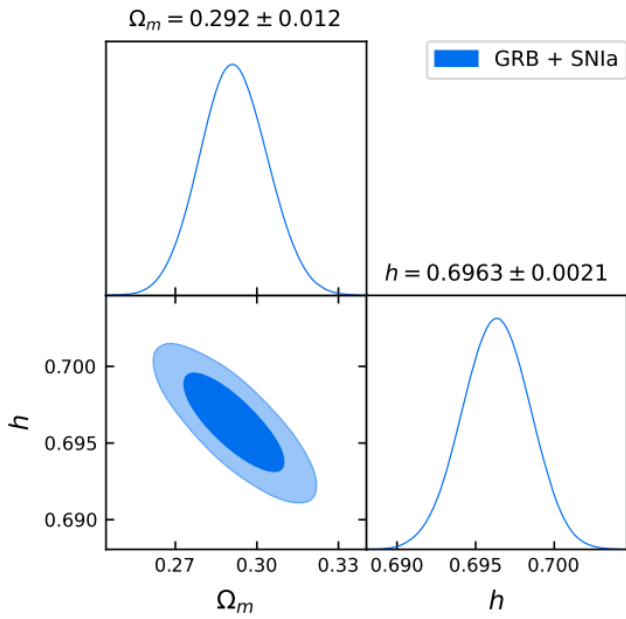


Figure 6. Joint constraints on parameters of Ω_m , h for the flat Λ CDM model with 98 GRBs ($z_i 1.4$) + 1048 SNe

compiled a long GRB sample from Swift and Fermi observations, which contains 221 long GRBs with redshifts from 0.03 to 8.20. Along with more and more GRBs observed from Fermi with much smaller scatters, GRBs could be used as an additional choice to set tighter constraints on cosmological parameters of DE models.

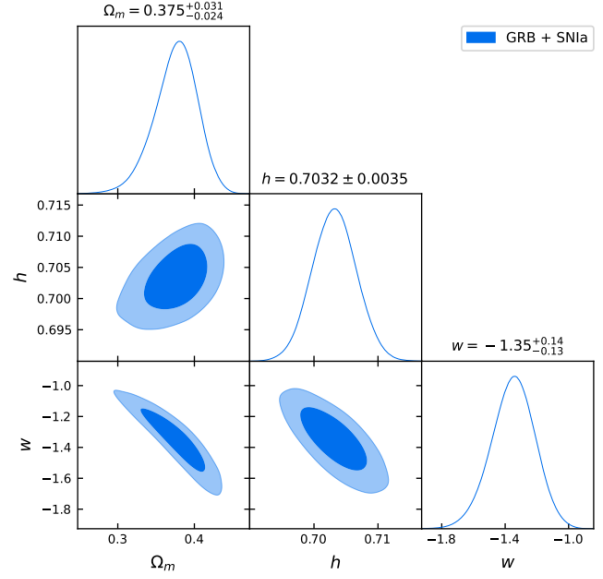


Figure 7. Joint constraints on parameters of Ω_m , h , and w_0 for the flat w CDM model with 98 GRBs ($z_i 1.4$) + 1048 SNe

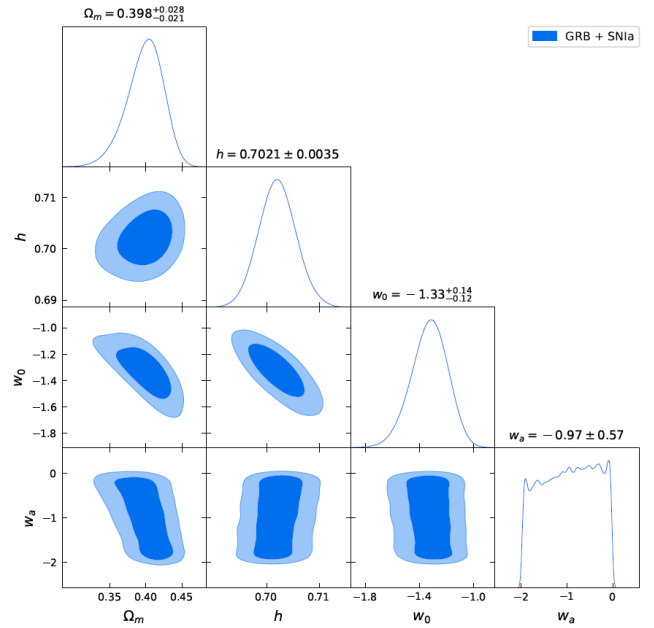


Figure 8. Joint constraints on parameters of Ω_m , h , w_0 and w_a for the flat CPL model with 98 GRBs ($z_i 1.4$) + 1048 SNe

ACKNOWLEDGMENTS

We thank Prof. Puxun Wu, Prof. Xiaoyao Xie, Prof. Jianchao Feng, Prof. Junjin Peng, Liu Yang, Xie Hanbei, XiaoDong Nong and Huifeng Wang for kind help and discussions. This project was supported by the Guizhou Provincial Science and Technology Foundation (QKHJC-ZK[2021] Key 020).

REFERENCES

- Akaike, H. 1974, *ITAC*, 19, 716
- Akaike, H. 1981, *J. Econ.*, 16, 3.
- Amati, L., D'Agostino, R., Luongo, O., Muccino, M., & Tantalò, M. 2019, *MNRAS*, 486, L46
- Amati, L., Frontera, F., Tavani, M., et al. 2002, *A&A*, 390, 81
- Amati, L., Guidorzi, C., Frontera, F., et al. 2008, *MNRAS*, 391, 577
- Benisty, D. 2021, *PDU*, 31, 100766
- Benisty, D., Mifsud, J., Levi Said, J., & Staicova, D. 2022, *arXiv:2202.04677*
- Borghi, N., Moresco, M. & Cimatti, A. 2022, *ApJL*, 928, L4
- Cao, S., Dainotti, M., & Ratra, B. 2022a, *MNRAS*, 512, 439
- Cao, S., Khadka, N., & Ratra, B. 2022b, *MNRAS*, 510, 2928
- Capozziello, S., & Izzo, L. 2008, *A&A*, 490, 31
- Capozziello, S. & Izzo, L. 2009, *NuPhS*, 194, 206
- Capozziello, S., & Izzo, L. 2010, *A&A*, 519, A73
- Capozziello, S., D'Agostino, R., & Luongo, O. 2018, *MNRAS*, 476, 3924
- Cardone, V. F., Capozziello, S., & Dainotti, M. G., 2009, *MNRAS*, 400, 775
- Chevallier, M. & Polarski, D. 2001, *IJMPD*, 10, 213
- Cucchiara, A., Levan, A., Fox, D. B., et al. 2011, *ApJ*, 736, 7
- D'Agostini, G. 2005, *arXiv: physics/0511182*
- Dainotti, M. G., Cardone V. F., & Capozziello S. 2008, *MNRAS*, 391, L79
- Dainotti, M. G., & Amati, L., 2018, *PASP*, 130, 051001
- Dainotti, M. G., Young, S., Li, L., et al. 2022a, *ApJS*, 261, 25
- Dai, Z., Liang, E., & Xu, D. 2004, *ApJ*, 612, L101
- Dai, Y., Zheng, X.-G., Li, Z. X., et al. 2021, *A&A*, 651, L8
- Demianski, M., & Piedipalumbo, E., 2011, *MNRAS*, 415, 3580
- Demianski, M., Piedipalumbo, E., Sawant, D., & Amati, L. 2017, *A&A*, 598, A112
- Demianski, M., Piedipalumbo, E., Sawant, D., & Amati, L. 2017, *A&A*, 598, A113
- Demianski, M., Piedipalumbo, E., Sawant, D., & Amati, L. 2021, *MNRAS*, 506, 903
- Fenimore, E. E., & Ramirez-Ruiz, E. 2000, *arXiv preprint astro-ph/0004176*
- Firmani, C., Ghisellini, G., Ghirlanda, G., & Avila-Reese, V. 2005, *MNRAS*, 360, L1
- Firmani, C., Ghisellini, G., Avila-Reese, V., & Ghirlanda, G. 2006, *MNRAS*, 370, 185
- Foreman-Mackey, D., Hogg, D. W., Lang, D., & Goodman, J. 2013, *PASP*, 125, 306
- Gao, H., Liang, N., & Zhu, Z.-H. 2012, *IJMPD*, 21, 1250016
- Ghirlanda, G., Ghisellini, G., & Lazzati, D. 2004a, *ApJ*, 616, 331
- Ghirlanda, G., Ghisellini, G., Lazzati, D., & Firmani, C. 2004b, *ApJ*, 613, L13
- Ghirlanda, G., Ghisellini, G., & Firmani, C. 2006, *New J. Phys.*, 8, 123
- Gomez-Valent, A. 2022, *PhRvD*, 105, 043528
- Gowri G. & Shantanu D. 2022, *JCAP*, 10, 069
- Hu, J. P., Wang, F. Y., & Dai, Z. G. 2021, *MNRAS*, 507, 730
- Izzo, L., Muccino, M., Zaninoni, E., Amati, L., & Della Valle, M. 2015, *A&A*, 582, A115
- Jia, X. D., Hu, J. P., Yang, J., Zhang, B. B., & Wang, F. Y. 2022, *MNRAS*, 516, 2575
- Jimenez, R., & Loeb, A. 2002, *ApJ*, 573, 37
- Jimenez, R., Verde, L., Treu, T. & Stern, D. 2003, *ApJ*, 593, 622
- Jiao, K., Borghi, N., Moresco, M. & Zhang, T.-J. 2022, *arXiv:2205.05701*
- Kessler, R., & Scolnic, D. 2017, *ApJ*, 836, 56
- Khadka, N. & Ratra, B. 2020, *MNRAS*, 499, 391
- Khadka, N., Luongo, O., Muccino, M., & Ratra, B. 2021, *JCAP*, 09, 042
- Kodama, Y., Yonetoku, D., Murakami, T., et al. 2008, *MNRAS*, 391, L1
- Liang, E., & Zhang, B. 2005, *ApJ*, 633, 611
- Liang, E., & Zhang, B. 2006, *MNRAS*, 369, L37
- Li, H., Xia, J.-Q., Liu, J., et al. 2008, *ApJ*, 680, 92
- Li, E.-K., Du, M., & Xu, L. 2020, *MNRAS*, 491, 4960
- Li, X., Keeley, R. E., Shafieloo, A., et al. 2021, *MNRAS*, 507, 919
- Liang, N., Xiao, W. K., Liu, Y., & Zhang, S. N. 2008, *ApJ*, 685, 354
- Liang, N., Wu, P., & Zhang, S. N. 2010, *PRD*, 81, 083518
- Liang, N., Xu, L., & Zhu, Z. H. 2011, *A&A*, 527, A11
- Liang, N., Li, Z., Xie, X., & Wu, P. 2022, *ApJ*, 941, 84
- Lin, H. N., Li, M. H., & Li, X. 2018, *MNRAS*, 480, 3117
- Linder, E. V. 2003, *PRL*, 90, 091301
- Liu, Y., Chen, F., Liang, N., et al. 2022, *ApJ*, 931, 50
- Liu, Y., Liang, N., Xie, X., et al. 2022, *ApJ*, 935, 7
- Liu, J., & Wei, H. 2015, *GRGr*, 47, 141
- Luongo, O., & Muccino, M. 2020, *A&A*, 641, A174
- Luongo, O., & Muccino, M. 2021, *MNRAS*, 503, 4581
- Luongo, O., & Muccino, M. 2023, *MNRAS*, 518, 2247(*arXiv:2207.00440*)
- Montiel, A., Cabrera, J. I., & Hidalgo, J. C. 2021, *MNRAS*, 467, 3239
- Moresco, M., Verde, L., Pozzetti, L., Jimenez, R. & Cimatti, A. 2012, *JCAP*, 2012, 053
- Moresco, M. 2015, 450, L16
- Moresco, M., Pozzetti, L., Cimatti, A. et al. 2016, *JCAP*, 2016, 014
- Moresco M., Jimenez R., Verde L., et al. 2020, *ApJ*, 898, 82
- Moresco M., Amati, L., Amendola, L. et al. 2022, *Living Reviews in Relativity*, 25, 6
- Muccino, M., Izzo, L., Luongo, O., et al. 2021, *ApJ*, 908, 181
- Muccino, M., Luongo, O., & Jain, D., 2022, *arXiv: 2208.13700*
- Norris, J. P., Marani, G. F., & Bonnell, J. T. 2000, *ApJ*, 534, 248
- Plank Collaboration. Aghanim, N., Akrami, Y., Arroja, F., et al. 2020, *A&A*, 641, A1
- Ratsimbazafy, A. L., Loubser, S. I., Crawford, S. M. et al. 2017, *MNRAS*, 467, 3239
- Schaefer, B. E. 2003, *ApJ*, 583, L67
- Schaefer, B. E. 2007, *ApJ*, 583, L67
- Scolnic, D. M., Jones, D. O., Rest, A., et al. 2018, *ApJ*, 859, 101
- Schwarz, G. 1978, *AnSta*, 6, 461
- Seikel, M., Clarkson, C., & Smith, M. 2012, *JCAP*, 06, 036
- Seikel, M., Yahya, S., Maartens, R., & Clarkson, C. 2012, *PRD*, 86, 083001
- Simon, J., Verde, L. & Jimenez, R. 2005, *PhRvD*, 71, 123001
- Stern, D., Jimenez, R., Verde, L., Kamionkowski, M. & Starford, S. A. 2010, *JCAP*, 2010, 008
- Tang L., Li X., Lin, H.-N., & Liu L. 2021, *ApJ*, 907, 121
- Tsutsui, R., Nakamura, T., Yonetoku, D., Murakami, T., Kodama, Y., & Takahashi, K. 2009, *JCAP*, 0908, 015
- Tsutsui, R., Nakamura, T., Yonetoku, D., et al. 2009, *MNRAS*, 394, L31
- Wang, F., & Dai, Z. G. 2006, *MNRAS*, 368, 371
- Wang, Y. 2008, *PhRvD*, 78, 123532
- Wang, F. Y., & Dai, Z. G. 2011, *A&A*, 536, 96
- Wang, J. S., Wang, F. Y., Cheng, K. S., & Dai, Z. G. 2016, *A&A*, 585, A68
- Wang, Y. Y., & Wang, F. Y. 2019, *ApJ*, 873, 39
- Wang, F. Y., Hu, J. P., Zhang, G. Q., & Dai, Z. G. 2022, *ApJ*, 924, 97
- Wei, H., Zhang, S. N. 2009, *EPJC*, 63, 139
- Wei, H., 2010, *JCAP*, 08, 020
- Xu, D., Dai, Z., & Liang, E. 2005, *ApJ*, 633, 603
- Xu, F., Tang, C.-H., Geng, J.-J., Wang, F.-Y., Wang, Y.-Y., Kuerban, A. & Huang, Y.-F. 2021, *ApJ*, 920, 135
- Yonetoku, D., Murakami, T., Nakamura, T., et al. 2004, *ApJ*, 609, 935
- Yu, B., Qi, S., & Lu, T. 2009, *ApJ*, 705, L15
- Zhang, C., Zhang, H., Yuan, S., Liu, S., Zhang, T. & Sun, Y. 2014, *RAA*, 14, 1221
- Zhang, J. C., Jiao, K., Zhang, T., Zhang, T. J., & Yu, B. 2022, *ApJ*, 936, 21

This paper has been typeset from a \LaTeX file prepared by the author.